microPET of Tumor Integrin $\alpha_v\beta_3$ Expression Using ^{18}F-Labeled PEGylated Tetrameric RGD Peptide (^{18}F-FPRGD4)

Zhanhong Wu*[1,2], Zi-Bo Li*[1], Kai Chen[1], Weibo Cai[1], Lina He[1], Frederick T. Chin[1], Fang Li[2], and Xiaoyuan Chen[1]

[1]*The Molecular Imaging Program at Stanford (MIPS), Department of Radiology and Bio-X Program, Stanford University School of Medicine, Stanford, California; and* [2]*Department of Nuclear Medicine, Peking Union Medical College Hospital, Beijing, China*

In vivo imaging of $\alpha_v\beta_3$ expression has important diagnostic and therapeutic applications. Multimeric cyclic RGD peptides are capable of improving the integrin $\alpha_v\beta_3$–binding affinity due to the polyvalency effect. Here we report an example of ^{18}F-labeled tetrameric RGD peptide for PET of $\alpha_v\beta_3$ expression in both xenograft and spontaneous tumor models. **Methods:** The tetrameric RGD peptide E{E[c(RGDyK)]$_2$}$_2$ was derived with amino-3,6,9-trioxaundecanoic acid (mini-PEG; PEG is poly(ethylene glycol)) linker through the glutamate α-amino group. NH_2-mini-PEG-E{E[c(RGDyK)]$_2$}$_2$ (PRGD4) was labeled with ^{18}F via the *N*-succinimidyl-4-^{18}F-fluorobenzoate (^{18}F-SFB) prosthetic group. The receptor-binding characteristics of the tetrameric RGD peptide tracer ^{18}F-FPRGD4 were evaluated in vitro by a cell-binding assay and in vivo by quantitative microPET imaging studies. **Results:** The decay-corrected radiochemical yield for ^{18}F-FPRGD4 was about 15%, with a total reaction time of 180 min starting from ^{18}F-F$^-$. The PEGylation had minimal effect on integrin-binding affinity of the RGD peptide. ^{18}F-FPRGD4 has significantly higher tumor uptake compared with monomeric and dimeric RGD peptide tracer analogs. The receptor specificity of ^{18}F-FPRGD4 in vivo was confirmed by effective blocking of the uptake in both tumors and normal organs or tissues with excess c(RGDyK). **Conclusion:** The tetrameric RGD peptide tracer ^{18}F-FPRGD4 possessing high integrin-binding affinity and favorable biokinetics is a promising tracer for PET of integrin $\alpha_v\beta_3$ expression in cancer and other angiogenesis related diseases.

Key Words: microPET; integrin $\alpha_v\beta_3$; tetrameric RGD peptide; PEGylation; ^{18}F

J Nucl Med 2007; 48:1536–1544
DOI: 10.2967/jnumed.107.040816

Integrins constitute an important family of transmembrane receptors involved in cell–cell or cell–matrix interactions and are central players in outside-in and inside-out signal transduction pathways (*1*). The $\alpha_v\beta_3$ heterodimer, which is not readily detectable in quiescent vessels but becomes highly expressed in angiogenic vessels and tumor cells, has been extensively studied (*2*). Integrin $\alpha_v\beta_3$ is necessary for the formation, survival, and maturation of newly formed blood vessels (*3*), and its expression correlates with tumor grade and histologic type in several cancer types, including melanoma, glioma, and ovarian and breast cancers (*4–6*). Thus, it would be highly advantageous to develop imaging agents that can be used to visualize and quantify integrin $\alpha_v\beta_3$ expression level, to more appropriately select patients considered for antiintegrin $\alpha_v\beta_3$ treatment, and to monitor antiintegrin treatment efficacy in $\alpha_v\beta_3$-positive patients.

Various imaging techniques—such as PET, SPECT, near-infrared fluorescence (NIRF) imaging, MRI, and ultrasound accompanied by appropriate imaging probes—have been applied to image integrin $\alpha_v\beta_3$ (*7–9*). For PET, Haubner et al. reported in 2001 that ^{18}F-galacto-RGD exhibited $\alpha_v\beta_3$-specific tumor uptake in an integrin-positive M21 melanoma xenograft model (*10*). Further tests in humans also indicated that the intensity of ^{18}F-galacto-RGD uptake correlates with $\alpha_v\beta_3$ expression (*11–14*). Recently, we and others found that dimeric and multimeric RGD peptides have significantly higher integrin affinity and, thus, significantly improved tumor targeting than the monomeric RGD analogs (*15–20*). For example, ^{18}F-fluorobenzoyl-E[c(RGDyK)]$_2$ (^{18}F-FB-E[c(RGDyK)]$_2$, denoted as ^{18}F-FRGD2), exhibited higher tumor uptake and more favorable in vivo pharmacokinetics than ^{18}F-FB-c(RGDyK) (^{18}F-FRGD) (*16,19*). It was hypothesized that the receptor binding of one RGD peptide significantly enhances the "local concentration" of the other RGD peptides in the vicinity of the receptor, which may lead to a faster rate of receptor binding or a slower rate of dissociation of radiolabeled RGD dimer from the integrin $\alpha_v\beta_3$, resulting in higher uptake and longer retention time in the tumor (*21*). Recently, we reported that ^{64}Cu-labeled tetrameric RGDfK peptide (^{64}Cu-DOTA-E{E[c(RGDfK)]$_2$}$_2$) had significantly higher tumor uptake and slower tumor washout rate compared with ^{64}Cu-labeled dimeric RGDfK peptide (^{64}Cu-DOTA-E[c(RGDfK)]$_2$) in a subcutaneous U87MG xenograft

Received Feb. 13, 2007; revision accepted Jun. 27, 2007.
For correspondence or reprints contact: Xiaoyuan Chen, PhD, The Molecular Imaging Program at Stanford (MIPS), Department of Radiology and Bio-X Program, Stanford University School of Medicine, 1201 Welch Rd., P095, Stanford, CA 94305-5484.
E-mail: shawchen@stanford.edu
*Contributed equally to this work.

model (*22*). It was also found that replacing D-Phe (f) with D-Tyr (y) increased the hydrophilicity of the RGD peptides and resulted in increased integrin $\alpha_v\beta_3$–mediated tumor uptake and more favorable biokinetics in an orthotopic MDA-MB-435 breast cancer model (*23*). On the basis of these findings, we believe that ^{18}F-labeled tetrameric RGDyK peptide (^{18}F-FB-E$\{$E[c(RGDyK)]$_2\}_2$, ^{18}F-FRGD4) might provide much higher receptor-binding affinity and tumor uptake than the corresponding dimeric and monomeric RGD peptide counterparts. However, because of the increased molecular size and spatial hindrance, direct labeling of RGD tetramer E$\{$E[c(RGDyK)]$_2\}_2$ with *N*-succinimidyl-4-^{18}F-fluorobenzoate (^{18}F-SFB) resulted in extremely low yield and, thus, was impractical for imaging applications.

In this study, we labeled PEGylated tetrameric RGD peptide NH_2-mini-PEG-E$\{$E[c(RGDyK)]$_2\}_2$ (PEG is poly (ethylene glycol)) with ^{18}F in reasonable yield and compared the tumor targeting efficacy and in vivo kinetics of the RGD tetramer with those of the RGD dimer analogs.

MATERIALS AND METHODS

All chemicals obtained commercially were of analytic grade and used without further purification. No-carrier-added ^{18}F-F$^-$ was obtained from an in-house PETtrace cyclotron (GE Healthcare). Reversed-phase extraction C-18 Sep-Pak cartridges were obtained from Waters and were pretreated with ethanol and water before use. The syringe filter and polyethersulfone membranes (pore size, 0.22 μm; diameter, 13 mm) were obtained from Nalge Nunc International. ^{125}I-Echistatin, labeled by the lactoperoxidase method to a specific activity of 74,000 GBq/mmol (2,000 Ci/mmol), was purchased from GE Healthcare. Analytic as well as semipreparative reversed-phase high-performance liquid chromatography (RP-HPLC) was performed on a Dionex 680 chromatography system with a UVD 170U absorbance detector and model 105S single-channel radiation detector (Carroll & Ramsey Associates). The recorded data were processed using Chromeleon version 6.50 software. Isolation of peptides and ^{18}F-labeled peptides was performed using a Vydac protein and peptide column (218TP510; 5 μm, 250 × 10 mm). The flow was set at 5 mL/min using a gradient system starting from 95% solvent A (0.1% trifluoroacetic acid [TFA] in water) and 5% solvent B (0.1% TFA in acetonitrile [ACN]) (0–2 min) and ramped to 35% solvent A and 65% solvent B at 32 min. The analytic HPLC was performed using the same gradient system, but with a Vydac column (218TP54, 5 μm, 250 × 4.6 mm) and a flow of 1 mL/min. The ultraviolet (UV) absorbance was monitored at 218 nm and the identification of the peptides was confirmed based on the UV spectrum acquired using a photodiode array detector.

Preparation of NH_2-Mini-PEG-E$\{$E[c(RGDyK)]$_2\}_2$ (PRGD4)

The E$\{$E[c(RGDyK)]$_2\}_2$ (denoted as RGD4) was prepared from cyclic RGD dimer E[c(RGDyK)]$_2$ according to our previously reported procedure (*17*). To a solution of Boc-11-amino-3,6,9-trioxaundecanoic acid (Boc-NH-mini-PEG-COOH, 40 mg, 0.13 mmol) and 20 μL *N,N*-diisopropylethylamine (DIPEA) in ACN was added *O*-(*N*-succinimidyl)-1,1,3,3-tetramethyl-uronium tetrafluoroborate (TSTU, 27 mg, 0.09 mmol). The reaction mixture was stirred at room temperature for 0.5 h and then added to E$\{$E[c(RGDyK)]$_2\}_2$ (10 mg, 3.6 μmol) in *N,N′*-dimethylformamide (DMF). The reaction was stirred at room temperature for another 2 h and the desired product, Boc-NH-mini-PEG-E$\{$E[c(RGDyK)]$_2\}_2$, was isolated by semipreparative HPLC. The collected fractions were combined and lyophilized to give a fluffy white powder (60% yield). The Boc-group was readily removed by treating Boc-NH-mini-PEG-E$\{$E[c(RGDyK)]$_2\}_2$ with anhydrous TFA for 5 min at room temperature. The crude product was purified by HPLC. The collected fractions were combined and lyophilized to afford NH_2-mini-PEG-E$\{$E[c(RGDyK)]$_2\}_2$ (denoted as PRGD4) as a white powder (90%). Analytic HPLC (retention time [R_t] = 13 min) and mass spectrometry (matrix-assisted laser desorption/ionization mass spectrometry [MALDI-TOF-MS]: m/z 3,001.0 for $[MH]^+$ ($C_{131}H_{194}N_{40}O_{42}$, calculated molecular weight [MW] 3,001.1)) confirmed the identity of the purified product.

Preparation of FB-NH-Mini-PEG-E$\{$E[c(RGDyK)]$_2\}_2$ (FPRGD4)

SFB (4 mg, 16.8 μmol) and PRGD4 (2 mg, 0.67 μmol) were mixed in 0.05 M borate buffer (pH 8.5) at room temperature. After 2 h, the desired product FB-NH-mini-PEG-E$\{$E[c(RGDyK)]$_2\}_2$ (denoted as FPRGD4) was isolated by semipreparative HPLC with a 65% yield. Analytic HPLC (R_t = 15.7 min) and mass spectrometry (MALDI-TOF-MS: m/z 3,123.4 for $[MH]^+$ ($C_{138}H_{197}FN_{40}O_{43}$, calculated [MW] 3,123.3) analyses confirmed product identification.

Radiochemistry

^{18}F-SFB was synthesized according to our previously reported procedure (*24*). Recently, we adapted the procedure into a commercially available synthesis module (GE TRACERlab FX_{FN}; GE Healthcare). The purified ^{18}F-SFB was rotary evaporated to dryness, reconstituted in dimethyl sulfoxide (DMSO; 200 μL), and added to a DMSO solution of PRGD4 (300 μg, 0.1 μmol) with DIPEA (20 μL). The peptide mixture was incubated at 60°C for 30 min. After dilution with 700 μL of water with 1% TFA, the mixture was purified by semipreparative HPLC. The desired fractions containing ^{18}F-FPRGD4 (Fig. 1) were combined and rotary evaporated to remove the solvent. ^{18}F-FPRGD4 was then formulated in normal saline and passed through a 0.22-μm Millipore filter into a sterile multidose vial for in vivo experiments.

Octanol–Water Partition Coefficient

Approximately 111 kBq of ^{18}F-FPRGD4 in 500 μL of phosphate-buffered saline (PBS, pH 7.4) were added to 500 μL of octanol in an Eppendorf microcentrifuge tube. The mixture was vigorously vortexed for 1 min at room temperature. After centrifugation at 12,500 rpm for 5 min in an Eppendorf microcentrifuge (model 5415R; Brinkman), 200-μL aliquots of both layers were measured using a γ-counter (Packard Instruments). The experiment was carried out in triplicates.

Cell Line and Animal Model

Animal procedures were performed according to a protocol approved by the Stanford University Institutional Animal Care and Use Committee. The U87MG tumor model was generated by subcutaneous injection of 5×10^6 cells into the front flank of female athymic nude mice (Harlan). The MDA-MB-435 tumor model was established by orthotopic injection of 5×10^6 cells into the left mammary fat pad of female athymic nude mice. The DU145 tumor model was established by subcutaneous injection of 5×10^6 cells into the left front flank of male athymic nude mice. The mice were subjected to microPET studies when the tumor

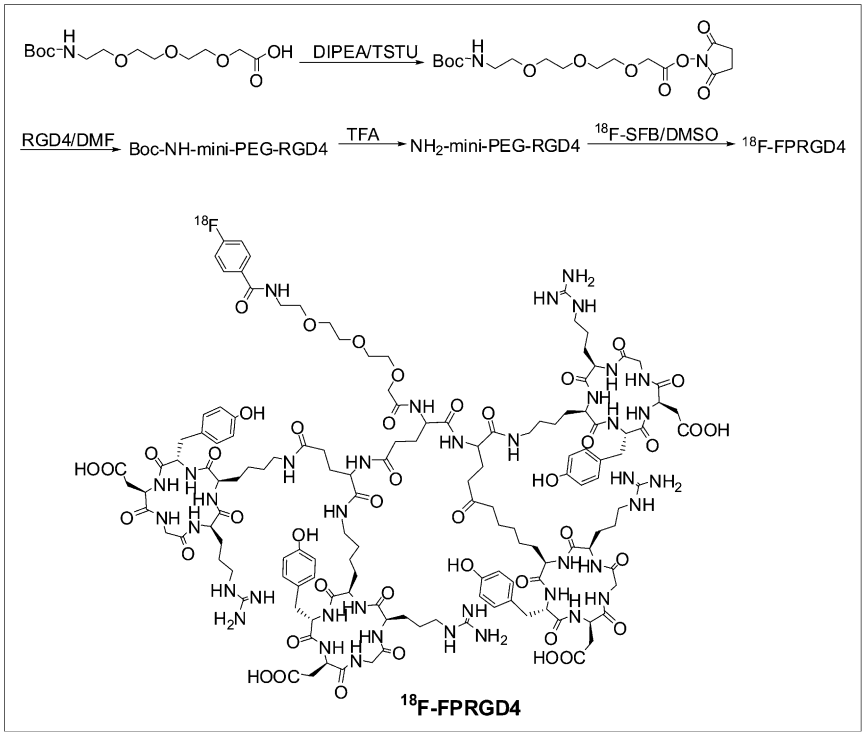

FIGURE 1. (Upper) Radiosynthesis scheme of ^{18}F-FPRGD4. (Lower) Chemical structure of ^{18}F-FPRGD4.

volume reached 100–300 mm^3 (3–4 wk after inoculation) (*20*). The c-neu oncomouse (Charles River Laboratories) is a spontaneous tumor-bearing model that carries an activated c-neu oncogene driven by a mouse mammary tumor virus (MMTV) promoter (*25*). Transgenic mice uniformly expressing the MMTV/c-neu gene develop mammary adenocarcinomas between 4 and 8 mo postpartum that involve the entire epithelium in each gland. These mice were subjected to microPET scans at about 8 mo of age, and the tumor volume was about 300–500 mm^3.

Cell Integrin Receptor-Binding Assay

In vitro integrin $\alpha_v\beta_3$–binding affinities and specificities of RGD4, PRGD4, and FPRGD4 were assessed via displacement cell-binding assays using ^{125}I-echistatin as the integrin $\alpha_v\beta_3$-specific radioligand. Experiments were performed on U87MG human glioblastoma cells by the method previously described (*17,20*). The best-fit 50% inhibitory concentration (IC_{50}) values for the U87MG cells were calculated by fitting the data with nonlinear regression using GraphPad Prism (GraphPad Software, Inc.). Experiments were performed with triplicate samples.

microPET Studies

PET scans and image analysis were performed using a microPET R4 rodent model scanner (Siemens Medical Solutions USA, Inc.) as previously reported (*17,19*). For the U87MG tumor model, mice (n = 3) were tail-vein injected with about 3.7 MBq (100 μCi) of ^{18}F-FPRGD4 under isoflurane anesthesia and then subjected to a 30-min dynamic scan (1 × 30 s, 4 × 1 min, 1 × 1.5 min, 4 × 2 min, 1 × 2.5 min, 4 × 3 min; total of 15 frames) starting 1 min after injection. Five-minute static PET images were also acquired at 1, 2, and 3 h after injection. The images were reconstructed by 2-dimensional ordered-subsets expectation maximization (OSEM) algorithm. No attenuation or scatter correction was applied. For the receptor-blocking experiment, a U87MG tumor mouse was coinjected with 10 mg/kg mouse body weight of c(RGDyK) and 3.7 MBq of ^{18}F-FPRGD4. The 5-min static PET scans was then acquired at 30 min and 1 h after injection. Multiple time-point static scans were also obtained for orthotopic MDA-MB-435, c-neu oncomouse, and subcutaneous DU145 tumor models after tail-vein injection with 3.7 MBq of ^{18}F-FPRGD4.

For each microPET scan, regions of interest (ROIs) were drawn over the tumor, normal tissue, and major organs by using vendor software (ASI Pro 5.2.4.0; Siemens Medical Solutions) on decay-corrected whole-body coronal images. The maximum radioactivity concentration (accumulation) within a tumor or an organ was obtained from mean pixel values within the multiple ROI volume, which were converted to counts/mL/min by using a conversion factor. Assuming a tissue density of 1 g/mL, the ROIs were converted to counts/g/min and then divided by the administered activity to obtain an imaging ROI–derived percentage injected dose per gram tissue (%ID/g).

Immunofluorescence Staining of c-neu Oncomice

Frozen tumor and organ tissue slices (5-μm thickness) were fixed with ice-cold acetone for 10 min and dried in air for 30 min. The slices were rinsed with PBS for 3 min and blocked with 10% goat serum for 30 min at room temperature. The slices were incubated with rat antimouse CD31 antibody (1:100; BD Biosciences) and hamster anti-β_3 antibody (1:100; BD Biosciences) for 3 h at room temperature and then visualized with Cy3-conjugated goat antihamster and fluorescein isothiocyanate (FITC)-conjugated goat antirat secondary antibody (1:200; Jackson ImmunoResearch Laboratories, Inc.).

Statistical Analysis

Quantitative data are expressed as mean ± SD. Means were compared using 1-way ANOVA and the Student t test. P values $<$ 0.05 were considered statistically significant.

RESULTS

Chemistry and Radiochemistry

The synthesis of RGD tetramer was performed through an active ester method by coupling Boc-Glu$(OSu)_2$ with dimeric RGD peptides followed by TFA deprotection. Boc-NH-mini-PEG-COOH was activated with TSTU/DIPEA and then conjugated with the amino group of tetrameric RGD peptide under a slightly basic condition. After TFA deprotection, PRGD4 was obtained as a fluffy white powder. The total synthesis time for ^{18}F-SFB was about 100 min and the decay-corrected yield was 67 ± 11% (n = 10) using the modified GE synthetic module (TRACERlab FX_{FN}). The decay-corrected radiochemical yield of ^{18}F-FPRGD4 based on ^{18}F-SFB was 22.0% ± 0.8% (n = 4). The radiochemical purity of ^{18}F-FPRGD4 was >99% according to analytic HPLC. The specific radioactivity of ^{18}F-FPRGD4 was determined to be about 100–200 TBq/mmol based on the labeling agent ^{18}F-SFB, as the unlabeled PRGD4 was efficiently separated from the product. Starting from ^{18}F-F^-, the total synthesis time of ^{18}F-FPRGD4, including the final HPLC purification, was about 180 min, and the overall decay-corrected yield was 15% ± 4%. In comparison, the yield of coupling $E\{E[c(RGDyK)]_2\}_2$ with ^{18}F-SFB was <2% (data not shown). The octanol–water partition coefficient (log$P$) for ^{18}F-FPRGD4 was −2.67 ± 0.22, which was slightly lower than ^{18}F-FRGD2 (−2.10 ± 0.03) and ^{18}F-FPRGD2 (−2.28 ± 0.05) (*26*).

In vitro Cell Integrin Receptor–Binding Assay

The receptor-binding affinity of RGD4, PRGD4, and FPRGD4 was determined by performing competitive displacement studies with ^{125}I-echistatin. All peptides inhibited the binding of ^{125}I-echistatin (integrin $\alpha_v\beta_3$ specific) to U87MG cells in a concentration-dependent manner. The IC_{50} values for RGD4, PRGD4, and FPRGD4 were 39.1 ± 5.5, 46.5 ± 5.3, and 37.7 ± 7.0 nM, respectively (n = 3) (supplemental Figs. S1–S3 are available online only at http://jnm.snmjournals.org; see supplemental Fig. S1). The comparable IC_{50} values of all 3 compounds suggest that insertion of the mini-PEG linker and fluorobenzoyl coupling had minimal effect on the receptor-binding affinity.

microPET of ^{18}F-FPRGD4 on Tumor-Bearing Mice

Dynamic microPET scans were performed on the U87MG xenograft model, and selected coronal images at different time points after injection of ^{18}F-FPRGD4 are shown in Figure 2A. The tumor was clearly visible with high contrast to contralateral background as early as 5 min after injection. Quantitation of tumor and major organ activity accumulation in microPET scans was realized by measuring ROIs encompassing the entire organ in the coronal orientation. The U87MG tumor uptake of ^{18}F-FPRGD4 was calculated to be 9.87 ± 0.10, 7.80 ± 0.14, 6.40 ± 0.27, 5.39 ± 0.14, and 4.82 ± 0.22 %ID/g at 5, 30, 60, 120, and 180 min after injection, respectively (n = 3). The averaged time–activity curves for the U87MG tumor, liver, kidneys, heart, lung, and muscle are shown in Figure 3. ^{18}F-FPRGD4 was cleared mainly through the kidneys. Some hepatic clearance was also observed.

Representative coronal microPET images of MDA-MB-435 tumor-bearing mice (n = 3) at different times after tracer injection are shown in Figure 2C. As the integrin expression level in MDA-MB-435 tumor is lower than that in U87MG, the tumor uptake of ^{18}F-FPRGD4 in MDA-MB-435 tumor (5.07 ± 0.18, 4.53 ± 0.36, and 3.38 ± 0.48 %ID/g at 30, 60, and 150 min after injection) was also lower than that in U87MG tumor. No significant difference in normal organs and tissues was found between these 2 tumor models.

^{18}F-FPRGD4 was also successful in visualizing a spontaneous murine mammary carcinoma model grown in c-neu oncomice (Fig. 2B) (*27–30*). The tumor uptakes were 4.22 ± 0.18, 3.56 ± 0.34, and 2.36 ± 0.40 %ID/g at 30, 60, and 150 min, respectively (n = 3). These values are slightly lower than those in MDA-MB-435 human breast cancer tumors grown in nude mice. No significant difference was found in major organs and tissues between the spontaneous tumor model of the BALB/c strain and the xenograft models of the nude mice strain.

We also tested ^{18}F-FPRGD4 in an integrin-negative DU145 tumor model (n = 3). As can be seen in Figure 2D, only slightly higher signal was detected in DU145 tumor (1.44 ± 0.34 and 0.93 ± 0.13 %ID/g at 30 and 60 min after injection) than the contralateral muscle background signal. These values were significantly lower than those in all 3 other integrin-expressing tumor models (P < 0.001). The tumor uptake followed the trend of U87MG > MDA-MB-435 > c-neu > DU145 (supplemental Fig. S2), which is consistent with the integrin $\alpha_v\beta_3$ expression pattern (quantified by $NaDodSO_4$-polyacrylamide/autoradiography) (*19*) in these tumor models (data not shown).

The integrin $\alpha_v\beta_3$ specificity of ^{18}F-FPRGD4 in vivo was also confirmed by a blocking experiment. Representative coronal images of U87MG tumor mice after injection of ^{18}F-FPRGD4 in the presence of a blocking dose of c(RGDyK) (10 mg/kg of mouse body weight) are illustrated in Figure 2E. More than 80% of the uptake in the tumor was inhibited as compared with that in the tumor without blocking (Fig. 2A). Radioactivity accumulation in most other major organs and tissues was also significantly reduced in the presence of nonradioactive RGD peptide.

The tumor uptake and biodistribution of ^{18}F-FPRGD4 derived from quantitative microPET were compared with those of the dimeric analog ^{18}F-FPRGD2 in the same U87MG tumor model (*26*). As shown in Figure 4, the uptake of ^{18}F-FPRGD4 in U87MG tumor was significantly higher than that of ^{18}F-FPRGD2 at all time points examined (P < 0.001). ^{18}F-FPRGD4 also showed higher uptake than that of ^{18}F-FPRGD2 in the liver and kidneys (P < 0.05). The initial muscle uptake of ^{18}F-FPRGD4 was higher than that of ^{18}F-FPRGD2 (P < 0.05), but the difference was diminished at late time points (P > 0.05).

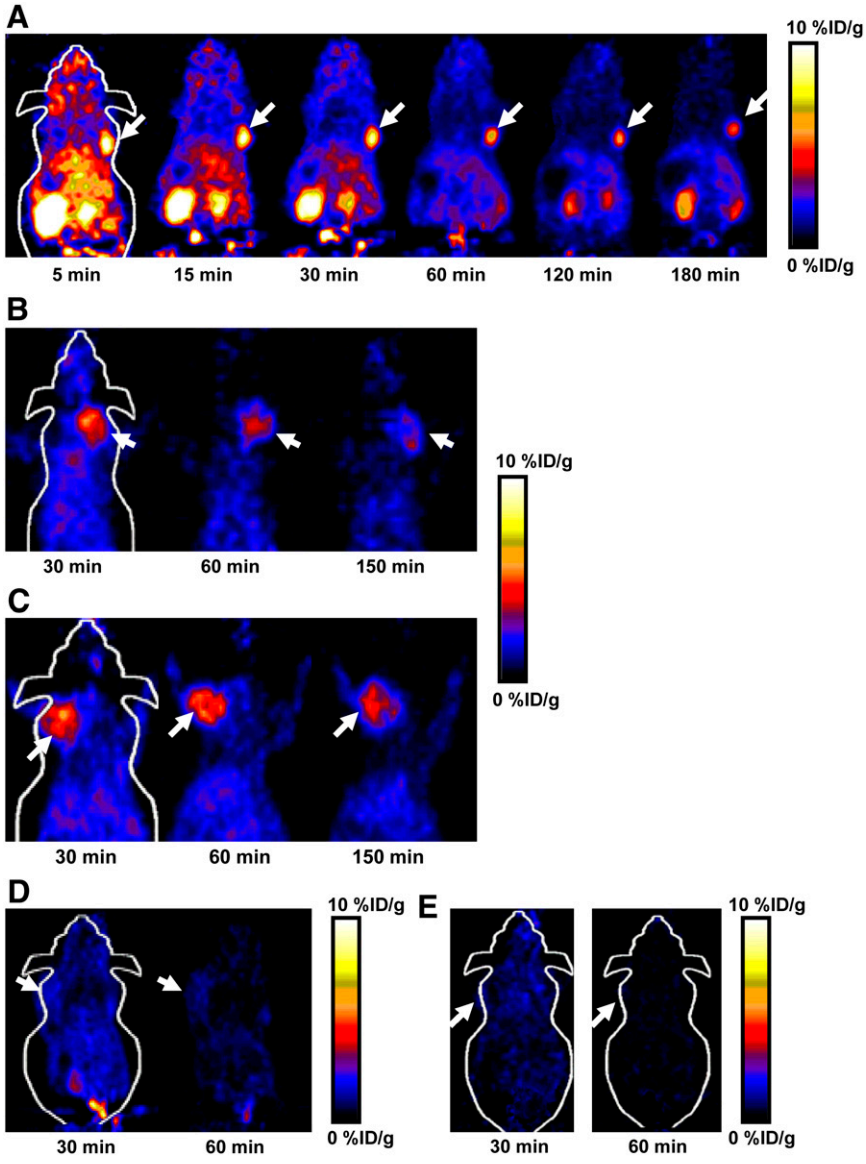

FIGURE 2. (A) Decay-corrected whole-body coronal microPET images of athymic female nude mice bearing U87MG tumor at 5, 15, 30, 60, 120, and 180 min after injection of ^{18}F-FPRGD4 (3.7 MBq [100 μCi]). (B) Decay-corrected whole-body coronal microPET images of c-neu oncomice at 30, 60, and 150min (5-min static image) after intravenous injection of ^{18}F-FPRGD4. (C) Decay-corrected whole-body coronal microPET images of orthotopic MDA-MB-435 tumor-bearing mouse at 30, 60, and 150 min after intravenous injection of ^{18}F-FPRGD4. (D) Decay-corrected whole-body coronal microPET images of DU-145 tumor-bearing mouse (5-min static image) after intravenous injection of ^{18}F-FPRGD4. (E) Coronal microPET images of a U87MG tumor-bearing mouse at 30 and 60 min after coinjection of ^{18}F-FPRGD4 and a blocking dose of c(RGDyK). Arrows indicate tumors in all cases.

Immunofluorescence Staining of c-neu Oncomice

The frozen tumor, liver, kidney, and lung tissue slices harvested from c-neu oncomice were stained for CD31 and mouse β_3-integrin. As can be seen in Figure 5, β_3-integrin was expressed in both tumor cells and endothelial cells of the murine mammary carcinoma, as most of the CD31-positive vessels were also β_3 positive. Integrin β_3 was also detected in the liver, lung, and kidneys. In particular, strong staining of integrin β_3 was found in the glomerulus, which might be partially responsible for high renal uptake of ^{18}F-FPRGD4. A similar integrin expression pattern was also seen in athymic nude mice (supplemental Fig. S3).

DISCUSSION

Various radiolabeled RGD peptides have been evaluated for tumor localization and therapy (*9,17,23,31*). However, most of the monomeric RGD peptide-based tracers developed so far have fast blood clearance accompanied by relatively low tumor uptake and rapid tumor washout, presumably due to the suboptimal receptor-binding affinity/selectivity and inadequate contact with the binding pocket located in the extracellular segment of integrin $\alpha_v\beta_3$. The natural functional mode of integrin binding involves multivalent interactions, which could provide not only more effective binding molecules but also systems that could improve the cell targeting and promote cellular uptake. Thus, we and others have applied the polyvalency principle (*15,22,31,32*) to develop dimeric and multimeric RGD peptides. We have labeled c(RGDyK) and E[c(RGDyK)]$_2$ with ^{18}F using ^{18}F-SFB as a prosthetic group (*16,20,32*). ^{18}F-FB-RGD (^{18}F-FRGD) had a good tumor-to-muscle ratio but rapid tumor washout and unfavorable hepatobiliary excretion, limiting its potential applications for imaging α_v-integrin–positive tumors in the lower abdomen area. In contrast, the dimeric RGD peptide tracer ^{18}F-FRGD2 had a

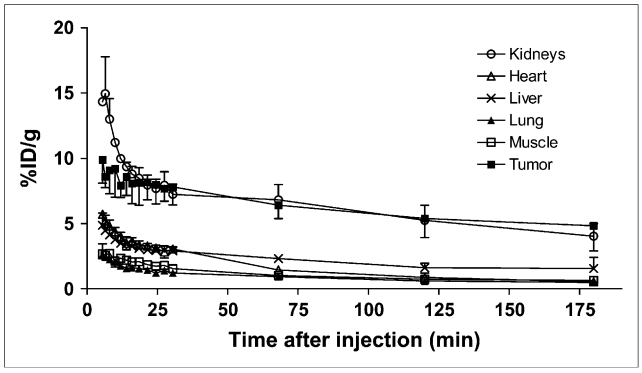

FIGURE 3. Time–activity curves of major organs after intravenous injection of ^{18}F-FPRGD4. Data were derived from a multiple time-point microPET study. ROIs are shown as the %ID/g ± SD (n = 3).

significantly higher tumor uptake and a prolonged tumor retention compared with ^{18}F-FRGD because of the synergistic effect of bivalency and improved pharmacokinetics (*20,32*). Thus, tetrameric RGD peptide tracer might be superior to the dimeric and monomeric peptide analogs due to the enhanced receptor binding caused by the polyvalency effect. However, the labeling yield of ^{18}F-FRGD4 was not satisfactory, due in part to the bulk of the 4 cyclic pentapeptides and the prosthetic group ^{18}F-SFB. The glutamate α-amine group has a pK_a of 9.47, which is also less reactive than the ε-amino group on the lysine side chain (pK_a = 8.95) usually used for ^{18}F labeling of peptides.

To overcome the problem of low labeling yield, we wanted to insert a PEG linker between the RGD tetramer and the prosthetic ^{18}F-labeling group. PEG moieties are inert, long-chain amphiphilic molecules produced by linking repeating units of ethylene oxide (*33*). PEGylation can decrease clearance, retain biologic activity, obtain a stable linkage, and enhance water solubility without significantly altering bioavailability (*34*). Moreover, PEG spacers are nontoxic and unreactive. PEGylation has been widely used for improving the in vivo kinetics of various pharmaceuticals (*27*). On the basis of previous studies (*16,32*), we found that PEGylated (MW 3,400) RGD peptides had lower integrin-binding affinity than non-PEGylated ones. Moreover, long-chain PEGs are mixtures of a broad range of different molecular weight compounds. Polydispersity of PEG complicates the characterization and quality control of the PEGylated compounds. In contrast, a mini-PEG spacer with definite molecular structure has been successfully used to reduce the spatial hindrance and improve the labeling yield for the dimeric RGD peptide (*26*). This PEGylation had minimal effect on the receptor-binding affinity, imaging quality, tumor uptake, and in vivo kinetics of dimeric RGD peptide $E[c(RGDyK)]_2$. Thus, we decided to use this strategy to make ^{18}F-labeled tetrameric RGD peptide. Indeed, the coupling yield between PRGD4 and ^{18}F-SFB was >20%, whereas the same reaction between RGD4 and ^{18}F-SFB was <2%. PRGD4 and FPRGD4 had an integrin-binding affinity similar to that of RGD4, demonstrating that mini-PEGylation had a minimal effect on the integrin affinity of this RGD tetramer.

The imaging quality of ^{18}F-FPRGD4 was tested in a U87MG human glioblastoma xenograft model, which has been well established to have high integrin expression. Compared with ^{18}F-FPRGD2, the tumor uptake of ^{18}F-FPRGD4 was >50% higher at all time points in the U87MG xenograft model (Fig. 4). No significant difference was observed in the tumor wash-out rate of ^{18}F-FPRGD4 and

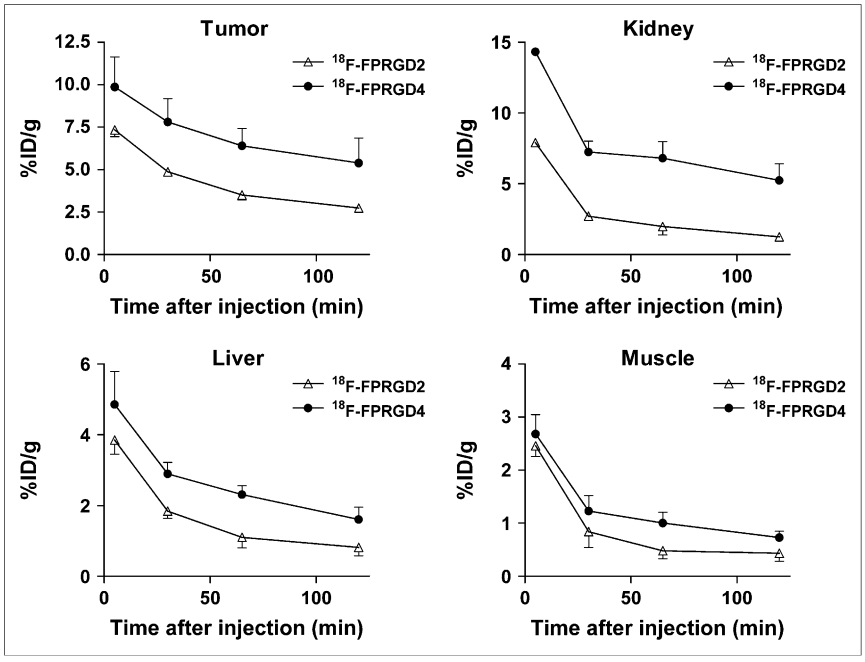

FIGURE 4. Comparison between uptake of ^{18}F-FPRGD2 and ^{18}F-FPRGD4 in U87MG tumor, kidneys, liver, and muscle over time. Data were derived from multiple time-point microPET study. ROIs are shown as %ID/g ± SD (n = 3).

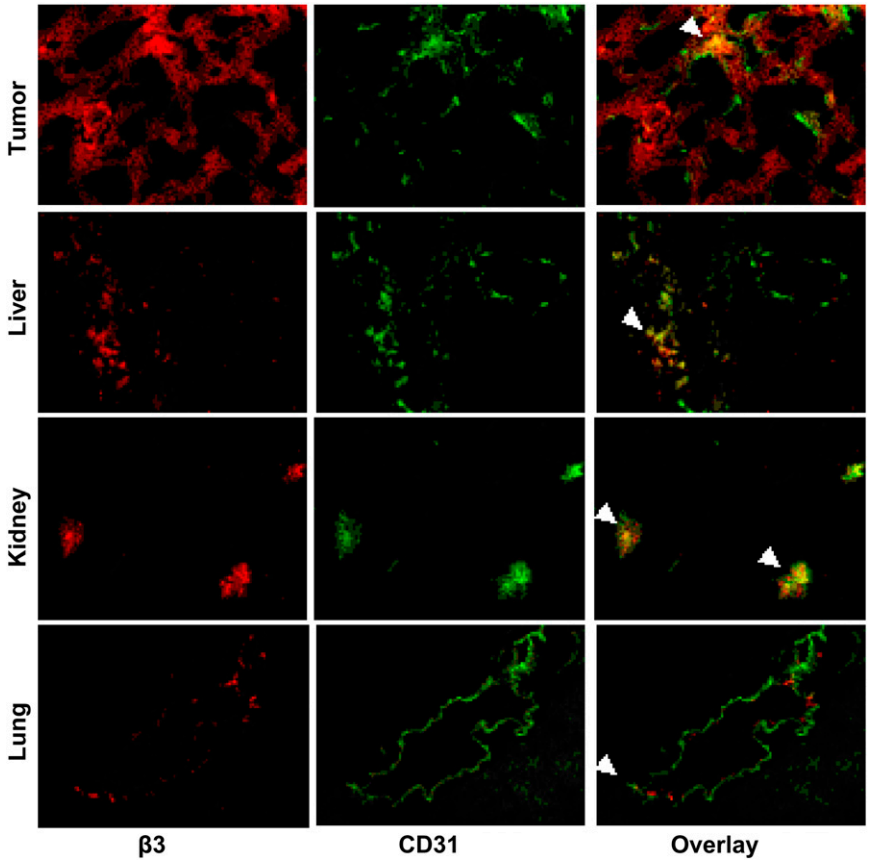

FIGURE 5. Immunofluorescent staining of β_3 and CD31 for tumor, liver, kidney, and lung. For β_3 staining, frozen tissue slices (5-μm thick) were stained with a hamster antimouse β_3 primary antibody and a Cy3-conjugated goat antihamster secondary antibody. For CD31 staining, frozen tissue slices were stained with a rat antimouse CD31 primary antibody and a FITC-conjugated goat antirat secondary antibody (×200). Arrowheads indicate overlay area in all cases.

^{18}F-FPRGD2. The increased uptake of ^{18}F-FPRGD4 than ^{18}F-FPRGD2 in the liver and kidneys may be due to the increased molecular size and some integrin expression in these organs. Since the tumor-to-nontumor ratios are similar when compared ^{18}F-FPRGD4 with ^{18}F-FPRGD2, further investigation is needed to determine whether the initial high tumor uptake is attributed to the high integrin affinity of ^{18}F-FPRGD4, or due to other factors such as enhanced circulatory half-life of the tetramer, molecular weight, and hydrophilicity. Overall, ^{18}F-FPRGD4 had significantly higher tumor uptake than, and comparable tumor/liver and tumor/muscle ratios ($P > 0.1$) with ^{18}F-FPRGD2. A similar pattern was also found for ^{64}Cu-labeled RGD peptides (*17*).

In the blocking experiment, nonradioactive RGD peptide inhibited the uptake of ^{18}F-FPRGD4 not only in U87MG tumor but also in several major organs (Fig. 2E). The biodistribution of ^{18}F-FPRGD4 (Figs. 3 and 4) showed initial rapid clearance of activity in the liver and kidney but then reached a plateau. These phenomena suggest that some normal organs and tissues may also be integrin positive, although to a less extent, as confirmed by immunohistochemistry. Immunohistopathology showed strong positive staining of the endothelial cells of the small glomeruli vessels in the kidneys and weak staining in the branches of the hepatic portal vein. However, other studies have shown that the kidney uptake of multimeric RGD peptides could also be caused by tubular reabsorption (*35*). Whether the higher renal uptake and retention of ^{18}F-FPRGD4 is integrin $\alpha_v\beta_3$-mediated is yet to be tested (*36*).

In this article, we inserted a mini-PEG linker to improve the labeling yield between ^{18}F-SFB and mini-PEGylated RGD tetramer. The coupling yield of slightly higher than 20% based on ^{18}F-SFB is still not satisfactory for routine clinical use. Furthermore, the synthesis of ^{18}F-SFB synthon is quite time consuming. Other ^{18}F-labeling strategies—such as click chemistry (*37*), reductive amination (*38*), Michael addition for thiol-specific coupling (*20*), and oxime formation (*39*)—may be utilized to simplify the labeling procedure and improve the labeling yield.

Although we have successfully demonstrated the specificity of ^{18}F-FPRGD4 for high (U87MG), medium (MDA-MB-435 and c-neu), and low (DU145) integrin $\alpha_v\beta_3$–expressing tumors, we did not determine whether the tumor-to-background contrast or the binding potential derived from Logan plot of the dynamic PET scans correlates well with the integrin expression level measured ex vivo by NaDodSO$_4$-PAGE/autoradiography or Western blot. Further characterizations of the metabolites in vivo might also provide more information about the ^{18}F-FPRGD4. Because of the enhanced receptor binding, we found that the tetrameric RGD peptide tracer ^{18}F-FPRGD4 showed significantly higher tumor uptake than its dimeric analog ^{18}F-FPRGD2. However, the ratios of tumor to muscle and tumor to major organ were similar. Thereby, appropriate

modification is needed to make it superior to the dimeric peptide analog ^{18}F-FPRGD2 and the monomeric peptide analogs (^{18}F-FRGD or ^{18}F-galacto-RGD). By replacing the mini-PEG linker with other pharmacokinetic modifiers, we may be able to modulate the overall molecular charge, hydrophilicity, and molecular size, thus possibly improving in vivo pharmacokinetics without compromising the tumor-targeting efficacy of the resulting radioconjugates. Moreover, the cost of tetrameric RGD peptides as compared to the dimeric and monomeric analogs cannot be ignored. More careful side-by-side comparisons among ^{18}F-FPRGD4, ^{18}F-FRGD2, and ^{18}F-galacto-RGD in human patients may be needed to assess the dosimetry and tumor-targeting sensitivity/specificity and, eventually, to identify the optimal RGD peptide tracer for PET imaging of integrin expression.

CONCLUSION

A new tetrameric RGD peptide tracer ^{18}F-FPRGD4 was designed and synthesized with good yield. Because of the polyvalency effect, this tracer showed high $\alpha_v\beta_3$-integrin–binding affinity and specificity in vitro. ^{18}F-FPRGD4 had much higher tumor uptake (6.40 ± 0.27 %ID/g at 60 min after injection) than the monomeric and dimeric RGD peptide analogs (3.80 ± 0.10 %ID/g for ^{18}F-FRGD and 3.40 ± 0.10 %ID/g for ^{18}F-FPRGD2 at 60 min after injection). The microPET studies performed in different tumor models suggest that ^{18}F-FPRGD4 may have great potential as a clinical PET radiopharmaceutical for imaging tumor integrin expression. The mini-PEG spacer (11-amino-3,6,9-trioxaundecanoic acid) is a suitable chemical means to modify the tumor-targeting ability and physiologic behavior of the tetrameric RGD peptide and can improve the radiolabeling yield using ^{18}F-SFB as a prosthetic group.

ACKNOWLEDGMENTS

This work was supported by National Institute of Biomedical Imaging and Bioengineering (NIBIB) (grant R21 EB001785), National Cancer Institute (NCI) (grants R21 CA102123, P50 CA114747, U54 CA119367, and R24 CA93862), Department of Defense (DOD) (grants W81XWH-04-1-0697, W81XWH-06-1-0665, W81XWH-06-1-0042, and DAMD17-03-1-0143), a Deans Fellowship from Stanford University and a Benedict Cassen Postdoctoral Fellowship from the Education and Research Foundation of the Society of Nuclear Medicine. We thank Dr. David W. Dick from the cyclotron facility for ^{18}F-F$^-$ production.

REFERENCES

1. Castel S, Pagan R, Mitjans F, et al. RGD peptides and monoclonal antibodies, antagonists of α_v-integrin, enter the cells by independent endocytic pathways. *Lab Invest.* 2001;81:1615–1626.
2. Cheng YF, Kramer RH. Human microvascular endothelial cells express integrin-related complexes that mediate adhesion to the extracellular matrix. *J Cell Physiol.* 1989;139:275–286.
3. Hwang R, Varner J. The role of integrins in tumor angiogenesis. *Hematol Oncol Clin North Am.* 2004;18:991–1006.
4. Albelda SM, Mette SA, Elder DE, et al. Integrin distribution in malignant melanoma: association of the β_3 subunit with tumor progression. *Cancer Res.* 1990;50:6757–6764.
5. Bello L, Francolini M, Marthyn P, et al. $\alpha_v\beta_3$ and $\alpha_v\beta_5$ integrin expression in glioma periphery. *Neurosurgery.* 2001;49:380–389; discussion 390.
6. Brooks PC, Stromblad S, Klemke R, Visscher D, Sarkar FH, Cheresh DA. Antiintegrin $\alpha_v\beta_3$ blocks human breast cancer growth and angiogenesis in human skin. *J Clin Invest.* 1995;96:1815–1822.
7. Cai W, Gambhir SS, Chen X. Multimodality tumor imaging targeting integrin $\alpha_v\beta_3$. *Biotechniques.* 2005;39:S6–S17.
8. Chen X. Multimodality imaging of tumor integrin $\alpha_v\beta_3$ expression. *Mini Rev Med Chem.* 2006;6:227–234.
9. Liu S. Radiolabeled multimeric cyclic RGD peptides as integrin $\alpha_v\beta_3$ targeted radiotracers for tumor imaging. *Mol Pharm.* 2006;3:472–487.
10. Haubner R, Wester HJ, Weber WA, et al. Noninvasive imaging of $\alpha_v\beta_3$ integrin expression using ^{18}F-labeled RGD-containing glycopeptide and positron emission tomography. *Cancer Res.* 2001;61:1781–1785.
11. Beer AJ, Haubner R, Goebel M, et al. Biodistribution and pharmacokinetics of the $\alpha_v\beta_3$-selective tracer ^{18}F-galacto-RGD in cancer patients. *J Nucl Med.* 2005;46:1333–1341.
12. Beer AJ, Haubner R, Sarbia M, et al. Positron emission tomography using ^{18}F-galacto-RGD identifies the level of integrin $\alpha_v\beta_3$ expression in man. *Clin Cancer Res.* 2006;12:3942–3949.
13. Beer AJ, Haubner R, Wolf I, et al. PET-based human dosimetry of ^{18}F-galacto-RGD, a new radiotracer for imaging $\alpha_v\beta_3$ expression. *J Nucl Med.* 2006;47:763–769.
14. Pichler BJ, Kneilling M, Haubner R, et al. Imaging of delayed-type hypersensitivity reaction by PET and ^{18}F-galacto-RGD. *J Nucl Med.* 2005;46:184–189.
15. Thumshirn G, Hersel U, Goodman SL, Kessler H. Multimeric cyclic RGD peptides as potential tools for tumor targeting: solid-phase peptide synthesis and chemoselective oxime ligation. *Chemistry (Easton).* 2003;9:2717–2725.
16. Chen X, Tohme M, Park R, Hou Y, Bading JR, Conti PS. Micro-PET imaging of $\alpha_v\beta_3$-integrin expression with ^{18}F-labeled dimeric RGD peptide. *Mol Imaging.* 2004;3:96–104.
17. Wu Y, Zhang X, Xiong Z, et al. microPET imaging of glioma integrin $\alpha_v\beta_3$ expression using ^{64}Cu-labeled tetrameric RGD peptide. *J Nucl Med.* 2005;46:1707–1718.
18. Chen X, Liu S, Hou Y, et al. MicroPET imaging of breast cancer α_v-integrin expression with ^{64}Cu-labeled dimeric RGD peptides. *Mol Imaging Biol.* 2004;6:350–359.
19. Zhang X, Xiong Z, Wu Y, et al. Quantitative PET imaging of tumor integrin $\alpha_v\beta_3$ expression with ^{18}F-FRGD2. *J Nucl Med.* 2006;47:113–121.
20. Cai W, Zhang X, Wu Y, Chen X. A thiol-reactive ^{18}F-labeling agent, N-[2-(4-^{18}F-fluorobenzamido)ethyl]maleimide, and synthesis of RGD peptide-based tracer for PET imaging of $\alpha_v\beta_3$ integrin expression. *J Nucl Med.* 2006;47:1172–1180.
21. Mammen M, Chio S-K, Whitesides GM. Polyvalent interactions in biological systems: implications for design and use of multivalent ligands and inhibitors. *Angew Chem Int Ed Engl.* 1998;37:2755–2794.
22. Cheng Z, Wu Y, Xiong Z, Gambhir SS, Chen X. Near-infrared fluorescent RGD peptides for optical imaging of integrin $\alpha_v\beta_3$ expression in living mice. *Bioconjug Chem.* 2005;16:1433–1441.
23. Chen X, Park R, Tohme M, Shahinian AH, Bading JR, Conti PS. MicroPET and autoradiographic imaging of breast cancer α_v-integrin expression using ^{18}F- and ^{64}Cu-labeled RGD peptide. *Bioconjug Chem.* 2004;15:41–49.
24. Chen X, Park R, Shahinian AH, et al. ^{18}F-Labeled RGD peptide: initial evaluation for imaging brain tumor angiogenesis. *Nucl Med Biol.* 2004;31:179–189.
25. Muller WJ, Sinn E, Pattengale PK, Wallace R, Leder P. Single-step induction of mammary adenocarcinoma in transgenic mice bearing the activated c-neu oncogene. *Cell.* 1988;54:105–115.
26. Wu Z, Li Z, Cai W, et al. ^{18}F-Labeled mini-PEG spacered RGD dimer (^{18}F-FPRGD2): synthesis and microPET imaging of $\alpha_v\beta_3$ integrin expression. *Eur J Nucl Med Mol Imaging.* May 5, 2007 [Epub ahead of print].
27. Harris TD, Kalogeropoulos S, Nguyen T, et al. Design, synthesis, and evaluation of radiolabeled integrin $\alpha_v\beta_3$ receptor antagonists for tumor imaging and radiotherapy. *Cancer Biother Radiopharm.* 2003;18:627–641.
28. Harris TD, Kalogeropoulos S, Nguyen T, et al. Structure-activity relationships of ^{111}In- and ^{99m}Tc-labeled quinolin-4-one peptidomimetics as ligands for the vitronectin receptor: potential tumor imaging agents. *Bioconjug Chem.* 2006;17:1294–1313.

29. Onthank DC, Liu S, Silva PJ, et al. ^{90}Y and ^{111}In complexes of a DOTA-conjugated integrin $\alpha_v\beta_3$ receptor antagonist: different but biologically equivalent. *Bioconjug Chem.* 2004;15:235–241.
30. Mousa SA, Mohamed S. Human $\alpha_v\beta_3$ integrin potency and specificity of TA138 and its DOTA conjugated form ^{89}Y-TA138. *J Cardiovasc Pharmacol.* 2005;45:109–113.
31. Janssen M, Oyen WJ, Massuger LF, et al. Comparison of a monomeric and dimeric radiolabeled RGD-peptide for tumor targeting. *Cancer Biother Radiopharm.* 2002;17:641–646.
32. Chen X, Hou Y, Tohme M, et al. Pegylated Arg-Gly-Asp peptide: ^{64}Cu labeling and PET imaging of brain tumor $\alpha_v\beta_3$-integrin expression. *J Nucl Med.* 2004; 45:1776–1783.
33. Harris JM, Martin NE, Modi M. Pegylation: a novel process for modifying pharmacokinetics. *Clin Pharmacokinet.* 2001;40:539–551.
34. Walsh S, Shah A, Mond J. Improved pharmacokinetics and reduced antibody reactivity of lysostaphin conjugated to polyethylene glycol. *Antimicrob Agents Chemother.* 2003;47:554–558.
35. Behr TM, Goldenberg DM, Becker W. Reducing the renal uptake of radiolabeled antibody fragments and peptides for diagnosis and therapy: present status, future prospects and limitations. *Eur J Nucl Med.* 1998;25:201–212.
36. Waldner C, Heise G, Meyer-Kirchrath J, Schror K, Grabensee B, Heering P. Selective cyclooxygenase-2 inhibition upregulates renal cortical alpha V integrin expression. *Nephron Exp Nephrol.* 2003;93:e72–e79.
37. Marik J, Sutcliffe JL. Click for PET: Rapid preparation of [^{18}F]fluoropeptides using Cu^{I} catalyzed 1,3-dipolar cycloaddition. *Tetrahedron Lett.* 2006;47:6881–6884.
38. Damhaut P, Cantineau R, Lemaire C, Plenevaux A, Christiaens L, Guillaume M. 2- and 4-[^{18}F]fluorotropapride, two specific D2 receptor ligands for positron emission tomography: N.C.A. syntheses and animal studies. *Int J Rad Appl Instrum [A].* 1992;43:1265–1274.
39. Poethko T, Schottelius M, Thumshirn G, et al. Two-step methodology for high-yield routine radiohalogenation of peptides: ^{18}F-labeled RGD and octreotide analogs. *J Nucl Med.* 2004;45:892–902.